Analysis of Recovery Time of Pt-, Pd-, and Au-Loaded SnO$_2$ Sensor Material with Nonanal as Large-Molecular-Weight Volatile Organic Compounds

Toshio Itoh,[1*] Daiheon Lee,[1,2†] Tomoyo Goto,[1††] Takafumi Akamatsu,[1]
Noriya Izu,[1] Woosuck Shin,[1] and Toshihiro Kasuga[1]

[1]National Institute of Advanced Industrial Science and Technology (AIST),
Shimo-shidami, Moriyama-ku, Nagoya, Aichi 463-8560, Japan
[2]Department of Frontier Materials, Nagoya Institute of Technology,
Gokiso-cho, Showa-ku, Nagoya, Aichi 466-8555, Japan

We investigated the recovery times of Pt-, Pd-, and Au-loaded SnO$_2$ (Pt, Pd, Au/SnO$_2$) semiconductor gas sensors after their exposure to nonanal as large-molecular-weight volatile organic compounds. The sensors were characterized by their response and temperature-programmed reaction (TPRe), and by transmission electron microscopy (TEM) observation. Sensors pretreated by sufficient aging showed good response but poor resistance recovery with nonanal, whereas good resistance recovery was observed with isoprene. The TPRe analysis revealed that aldehyde gas molecules were oxidized to carboxylic acids on the sensors at the sensor working temperature. In sufficiently aged Pt, Pd, and Au/SnO$_2$ sensors, the loaded Pt, Pd, and Au catalysts were observed to aggregate by TEM. From these results, we suggest different dispersion states of the loaded Pt, Pd, and Au noble metal particles, the mechanism of oxidation and adsorption of nonanal molecules on SnO$_2$ grain surface, and their relationship to the recovery time after exposure to nonanal.

1. Introduction

Metal-oxide semiconductors, such as SnO$_2$, are among the most suitable materials for resistive sensors for volatile organic compounds (VOCs).[1,2] Oxygen molecules from the air adsorb on the surface of SnO$_2$ and remove electrons from the conduction band of SnO$_2$, giving rise to an electron-depletion layer, which acts as a potential barrier between neighboring grains.[3,4] The resistivity of the sensor element depends on the change in the thickness of the electron-depletion layer. In the presence of VOC molecules, the electron-depletion layer becomes thinner because of the oxidation of VOCs by the oxygen adsorbates. Thus, the oxidation of VOCs is key to the functioning of SnO$_2$ semiconductor gas sensors. The gas sensing properties of SnO$_2$-type sensors (i.e., selectivity and sensitivity) can be controlled by the addition of noble metal catalysts, and their sensitivity also depends on the functional groups present in the target gases. For instance, pristine SnO$_2$ shows high

---

*Corresponding author: e-mail: itoh-toshio@aist.go.jp
†Present appress: Department of Chemistry, Korea Advanced Institute of Science and Technology (KAIST), Daehak-ro, Yuseong-gu, Daejeon 34141, Korea
††Present appress: The Institute of Scientific and Industrial Research (ISIR), Osaka University, 8-1 Mihogaoka, Ibaraki, Osaka 567-0047, Japan

response to oxy-hydrocarbons such as alcohols but low response to other VOCs.[5,6] We previously reported a Pt-, Pd-, and Au-loaded SnO_2 (Pt, Pd, Au/SnO_2) material for use in total VOC sensors.[5–8] The loading of the noble metals, Pt, Pd, and Au, effectively improved the sensitivity to aliphatic, halogenated, and aromatic hydrocarbons, respectively.[5,6] The Pt, Pd, Au/SnO_2 sensors with all three noble metals are therefore suitable for the detection of diverse VOCs.

VOCs in breath air are known to be related to halitosis,[9–11] metabolism,[12–15] and diseases[16–20] in the human body. Hence, VOC sensors are desirable for monitoring the concentrations of VOCs in breath air. As an example, the isoprene and acetone concentrations in breath air are related to metabolism,[12–15] and aldehydes are included in the breath of lung cancer patients. Fuchs *et al*. reported that the breath of lung cancer patients includes higher concentrations of pentanal, hexanal, octanal, and nonanal than those of healthy controls.[17] The median concentrations of three aldehyde gases, such as pentanal, hexanal, and octanal, from the breath of lung cancer patients were too small (at the sub ppb level) to be detected by semiconductive metal oxide gas sensors. However, the median concentration of nonanal was several ppb. VOCs at ppb-level concentrations can be detected by metal oxide sensors with adsorbents as gas condensing units. Therefore, it is important to improve the nonanal-sensing properties of metal oxide-type sensors such as Pt, Pd, Au/SnO_2. For developing the Pt, Pd, Au/SnO_2-type gas sensors for breath analysis, we have investigated ways of improving their sensitivity by pretreatment, that is, by prolonged aging at the sensor working temperature.[21] The pretreatment enhances the resistance decrease of the Pt, Pd, Au/SnO_2 sensors during exposure to nonanal, but it also decreases the resistance recovery rate after the exposure. The effects of aging on noble metal catalysts such as Pt and Pd have been reported.[22–24] However, a clear relationship between the conditions of noble metal catalysts and the gas sensing properties of the corresponding SnO_2-type systems has not been reported.

In this study, we investigate the effects of pretreatment on the recovery time of the Pt, Pd, Au/SnO_2 sensors after exposure to nonanal as high-molecular-weight VOCs. Repeated exposure measurements on Pt, Pd, Au/SnO_2 sensors to nonanal were performed in order to investigate changes in the sensing properties. We also investigated the chemical reaction mechanism of nonanal on the surface of the sensor materials using the temperature-programmed reaction (TPRe). The relationship between the sensing properties and the dispersibility of the noble metals in non-aged and aged Pt, Pd, Au/SnO_2 systems was examined by transmission electron microscopy (TEM) as well as by scanning TEM with high-angle annular dark field (STEM-HAADF), and STEM with energy-dispersive spectroscopy (STEM-EDS).

2. Materials and Methods

2.1 Preparation of sensor elements

The Pt, Pd, Au/SnO_2 sensor elements were prepared according to our previous report.[21] Before the preparation of thick films of sensing materials, a platinum comb-type electrode 7.5 mm^2 in area with a 10 µm gap and 10 µm line width was formed on a 4 × 4 mm^2 surface-oxidized Si substrate, and a Pt heater was patterned on the backside of the substrate. Pt (particle size: 2 nm), Pd (particle size: 4 nm), and Au (particle size: 3 nm) colloid suspensions (Tanaka Kikinzoku Kogyo K.K.) were added to SnO_2 powder (particle size: <100 nm; Aldrich) at 1 wt% each relative to SnO_2. The mixtures were stirred and dried, and subsequently heated at 400 °C for 2 h. The resulting powder is abbreviated as "Pt, Pd, Au/SnO_2". The Pt, Pd, Au/SnO_2 powder was combined with an

ethylcellulose-type organic dispersant to obtain a paste. The powder/vehicle ratio of the paste was 1/16. The paste was subsequently applied to the prepared substrate with a platinum comb-type electrode using a Musashi Engineering FAD-320s dispenser. The substrate was then dried at 80 °C for 2 h, and annealed at 500 °C for 2 h in room air. The Pt, Pd, Au/SnO$_2$ thick film was obtained. The resulting sensor element was mounted on a dedicated stem, as shown in Fig. 1. After that, the elements were maintained at 300 °C for 3 d in room air for aging, i.e., the pretreatment, using their Pt heater.

Simultaneously, another Pt, Pd, Au/SnO$_2$ thick film was prepared in the same manner. The thick film was broken, and the edge section was observed by a field emission scanning electron microscope for measuring the film thickness, which was approximately 4 mm.

2.2 Sensor response measurement

The gas sensing properties of the elements were measured using a flow-type gas sensing apparatus. The elements were placed in a tubular sample chamber. Nonanal and isoprene were used as target gases, whose concentrations were controlled to be 0.055–9.5 and 0.13–2.5 ppm, respectively. The chemical structures of nonanal and isoprene are shown in Fig. 2. Nonanal gas was generated from a liquid source using the gas generator PD-1B "permeater" (Gastec Corporation, Japan). Isoprene gas was prepared by diluting the standard cylinder gas of 50 ppm isoprene (Sumitomo Seika Chemicals). The total flow rate in the chamber was kept at 200 mL/min. First, pure air was flowed, then nonanal or isoprene gas was flowed for 3 or 5 min, and finally, the flow was changed back to pure air. The sensing experiments of nonanal (N) and isoprene (I) were carried out in the sequence of I-I-I-I-I-N-I-I-N-N-I. The first nonanal sensing was carried out between the fifth and sixth isoprene sensing analyses, while the second and third nonanal analyses were carried out between the seventh and eighth isoprene analyses. Sensing analyses were carried out at the sensor working temperature of 250 °C. The sensor response value (*S*) is defined as
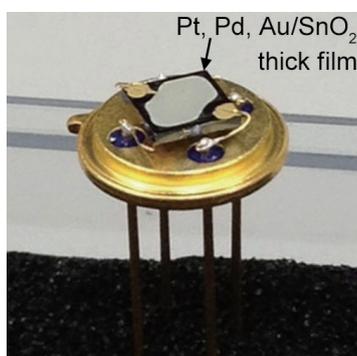
$$S = \frac{R_a}{R_g}, \tag{1}$$

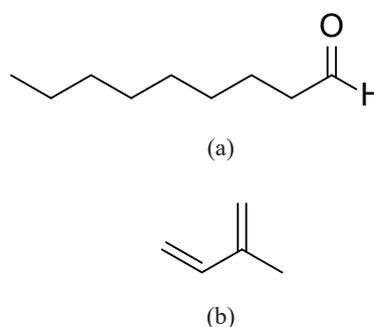Fig. 1.   (Color online) A prepared Pt, Pd, Au/SnO$_2$ sensor element.

Fig. 2.   Structural formulas of the target gases: (a) nonanal and (b) isoprene.

where R_a and R_g are the electrical resistances in pure air and nonanal or isoprene, respectively. The resistance recovery time (t_{10}) is defined as the time required to reach a 10%-reduced resistance from R_a after switching from target gas (nonanal or isoprene) to pure air. If the resistance does not reach the 10%-reduced resistance from R_a after 300 s, the resistance recovery rate $P(t)$ at $t = 300$ s, i.e., $P(300)$, is used instead of t_{10}. $P(t)$ is definied as

$$P(t) = \frac{R(t) - R_g}{R_a - R_g} \times 100 \ (\%), \qquad (2)$$

where $R(t)$ is resistance at t, which is the time from the switch to pure air.

2.3 Temperature programmed reaction analysis

In the TPRe study, butyraldehyde was used as the target gas, and the corresponding gas sensing property of Pt, Pd, Au/SnO$_2$ was compared with that using nonanal. Moreover, butyric acid (the oxidization product of butyraldehyde) was also used as a target gas. 8.8–30 ppm butyraldehyde and 0.31–1.6 ppm butyric acid gases were used.

The TPRe analysis was carried out according to Sakurai et al.,[25] using a flow-type gas reaction measurement apparatus equipped with a Canon Anelva quadrupole mass spectrometer (MS) M-201QA. Figure 3 shows the flow apparatus for the TPRe analysis. Twenty milligram of Pt, Pd, Au/SnO$_2$ or SnO$_2$ powder annealed at 500 °C was mixed with 500 mg of quartz sand to prevent clogging of the flow stream. The mixture powder was put in a quartz tube using glass wool. In the TPRe study, 1.8×10^3 ppm butyraldehyde and 2.0×10^3 ppm isoprene were used as target gases. Butyraldehyde was generated from a liquid source by the PD-1B "permeater", while isoprene was prepared by 1% isoprene with helium gas (Sumitomo Seika Chemicals). The total flow rate was 200 mL/min, and the He/O$_2$ ratio was 4. The gas was flowed through a quartz tube and exposed to the Pt, Pd, Au/SnO$_2$ or pristine SnO$_2$ powder. The quartz tube was heated from room temperature to 500 °C at the heating rate of 5 °C/min. The MS spectra were recorded with the sample powder temperature from 120 to 500 °C for analyzing the constituents of the exhaust flow gas.
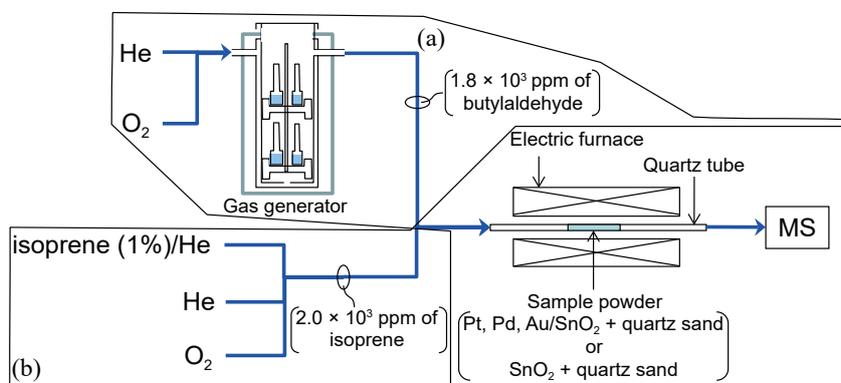

Fig. 3. (Color online) Schematic diagram of flow apparatus used for the TPRe analysis. The target gases were (a) 1.8×10^3 ppm butylaldehyde and (b) 2.0×10^3 ppm isoprene.

2.4   TEM observations

For the TEM samples, Pt, Pd, Au/SnO$_2$ paste was applied to two identical substrates, dried, and then annealed at 500 °C for 2 h in room air. Afterwards, the Pt, Pd, Au/SnO$_2$ thick film of one sample was scraped off the substrate and pulverized. The obtained powder was called "non-aged Pt, Pd, Au/SnO$_2$". The other sample was held at 300 °C for 13 d in room air and exposed to 9.5 ppm nonanal for around 1 d, in order to approximate the aging and nonanal sensing processes, respectively. Subsequently, this thick film was also scraped off and pulverized, and the powder was called "aged Pt, Pd, Au/SnO$_2$". The two powders were observed on a FEI Tecnai Osiris TEM instrument.

3.   Results and Discussion

3.1   Sensor responses to nonanal and isoprene

The first nonanal analysis was carried out after the fifth isoprene analysis. Figure 4(a) shows the dynamic resistance responses of the Pt, Pd, Au/SnO$_2$ element to nonanal. The resistance drastically decreased upon exposure to nonanal, and the sensor response value at the first application of nonanal (9.5 ppm) was 47. After this exposure to nonanal, the resistance did not return to within
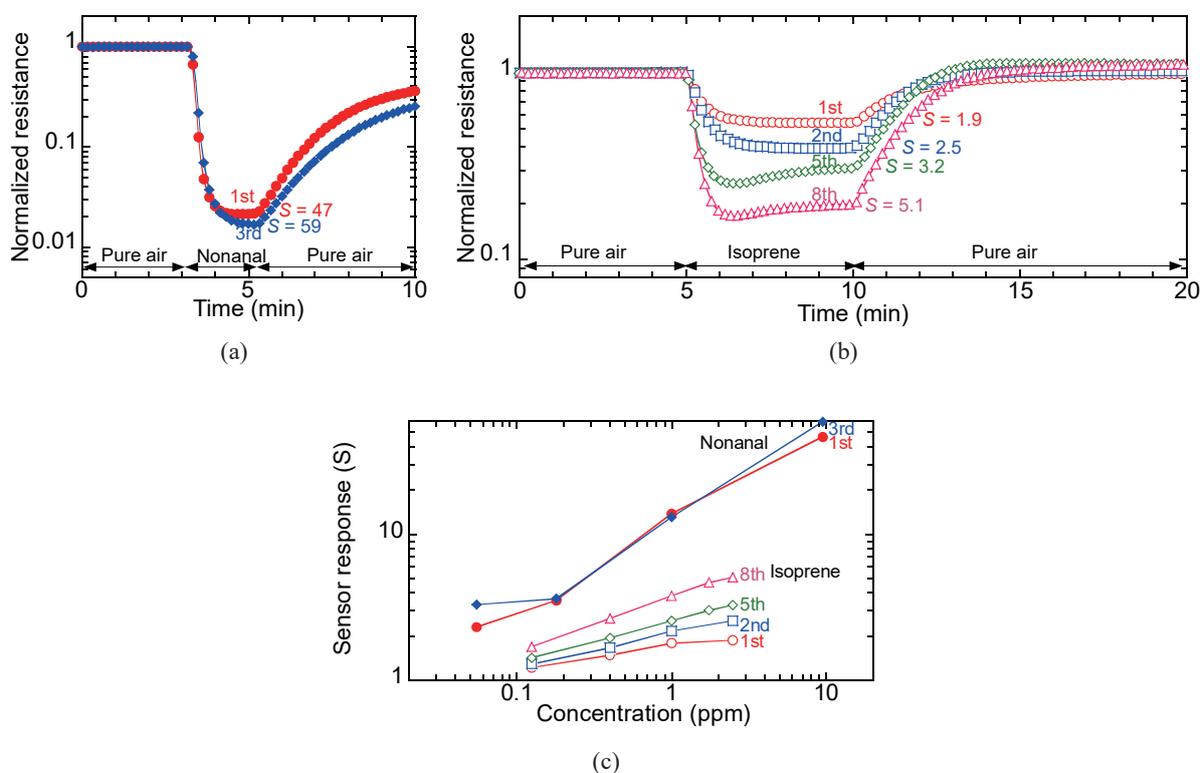

Fig. 4.   (Color online) Dynamic resistance responses of the Pt, Pd, Au/SnO$_2$ sensor element to (a) 9.5 ppm nonanal and (b) 2.5 ppm isoprene, and (c) sensor response values *S* with different target gases and concentrations. The temperature of the sensor element was 250 °C.

90% of its original value in 300 s, as shown in Table 1. In our previous study, nonanal was also tested on the non-aged Pt, Pd, Au/SnO$_2$ sensor,[21] where the sensor response value was also low (S = 17) at 250 °C, and sufficient resistance recovery was observed within 300 s. In this study, the sensor response value of the third nonanal analysis, after the seventh isoprene analysis, was slightly better than that of the first. However, the recovery rate [$P(t)$] of resistance was worse than the first time [$P(300)$ = 24 vs 34%], as shown in Table 1.

Figure 4(b) shows the dynamic resistance responses of the aged Pt, Pd, Au/SnO$_2$ element to isoprene. The resistance was decreased by exposure to isoprene, and the sensor response value of the first 2.5 ppm isoprene analysis was 1.9. In subsequent repeated isoprene sensing, S gradually increased (S = 3.2 at the fifth and 5.1 at the eighth), indicating that the gas sensing analysis also induced further aging of the Pt, Pd, Au/SnO$_2$ sensor elements. After exposure to isoprene, the resistance reached the 10%-reduced resistance from R_a within 300 s, as shown in Table 1. The recovery of resistance in the aged Pt, Pd, Au/SnO$_2$ sensor after exposure to isoprene was almost at the same level as that of the non-aged Pt, Pd, Au/SnO$_2$ after exposure to nonanal (t_{10} = 212–374 vs 120 s).

The third nonanal analysis was carried out just before the eighth isoprene analysis. The sensor response value of the third nonanal analysis at 0.18 ppm (S = 3.6) is almost the equal to that of the eighth 1.0 ppm isoprene analysis (3.8), as shown in Fig. 5. However, the recovery of resistance was much slower after exposure to nonanal [t_{10} > 300 s; $P(300)$ = 32] than that of isoprene (t_{10} = 212 s), as shown in Table 1.

Table 1
Sensor response value (S), resistance recovery time (t_{10}), and recovery rate [$P(t)$] of the Pt, Pd, Au/SnO$_2$ sensor element under different conditions.

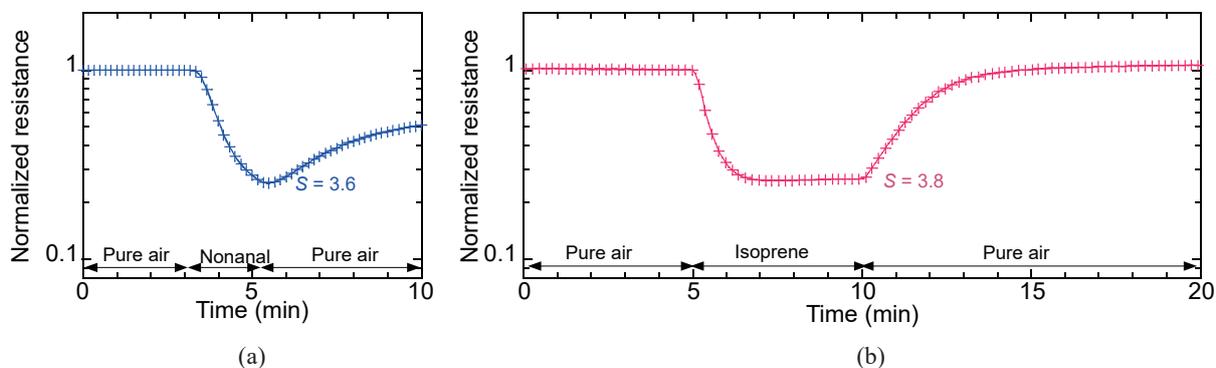| Condition	Target gas	S	t_{10} [s]	$P(300)$ [%]
Aged	9.5 ppm nonanal-1st [Fig. 3(a)]	47	>300	34
Aged	9.5 ppm nonanal-3rd [Fig. 3(a)]	59	>300	24
Aged	0.18 ppm nonanal-3rd [Fig. 3(a)]	3.6	>300	31
Aged	2.5 ppm isoprene-1st [Fig. 3(b)]	1.9	374	87
Aged	2.5 ppm isoprene-5th [Fig. 3(b)]	3.2	145	—
Aged	2.5 ppm isoprene-8th [Fig. 3(b)]	5.1	212	—
Aged	1.0 ppm isoprene-8th [Fig. 3(b)]	3.8	212	—
Non-aged[21]	9.5 ppm nonanal	17	120	—

Fig. 5. (Color online) Dynamic resistance response of the Pt, Pd, Au/SnO$_2$ sensor element to (a) 0.18 ppm nonanal on the third analysis and (b) 1.0 ppm isoprene on the eighth analysis. The temperature of the sensor element was 250 °C.

3.2   Results of TPRe analysis

The MS in the TPRe instrument can detect ionized molecules that possess *m/z* (ratio between atomic mass and positive charge) from 1 to 100; therefore, the molecular ion of nonanal [$M(C_8H_{17}CHO)$ = 142.2] cannot be detected. Also, the recommended concentration analyzed by MS is several thousand ppm, which could not be achieved for nonanal owing to its low vapor pressure. We therefore used butyraldehyde [$M(C_3H_7CHO)$ = 72.1] instead of nonanal in the TPRe study. In order to validate this substitution, the sensing property of the sensors with butyraldehyde was compared with that with nonanal before the TPRe study. Prior to butyraldehyde and nonanal sensing, the Pt, Pd, Au/SnO$_2$ sensor element had also been aged at 300 °C for 3 d in room air, followed by its use for sensing analysis on several target gases countless times. Therefore, this sensor is called the "advanced-aging" Pt, Pd, Au/SnO$_2$ element.

Figure 6(a) shows the dynamic resistance responses of the Pt, Pd, Au/SnO$_2$ element to 9.5 ppm nonanal, 8.8 ppm butyraldehyde, and 1.6 ppm butyric acid (the product of butyraldehyde oxidization). From Fig. 6(a), Pt, Pd, Au/SnO$_2$ showed almost the same resistance responses to nonanal and butyraldehyde at similar concentrations. Therefore, the main sensor response mechanism would involve the aldehyde group rather than the alkyl chain. The resistance recovery rate after butyraldehyde exposure was better than that after nonanal exposure, as shown in Table 2, indicating that the recovery rate is related to the desorption of target gas molecules from the SnO$_2$ system, because butyraldehyde has a lower molecular weight than nonanal. The resistance recovery rate after exposure to butyric acid was lower than that after exposure to butyraldehyde, even though the concentration of butyric acid (1.6 ppm) was lower than that of butyraldehyde (8.8 ppm), as
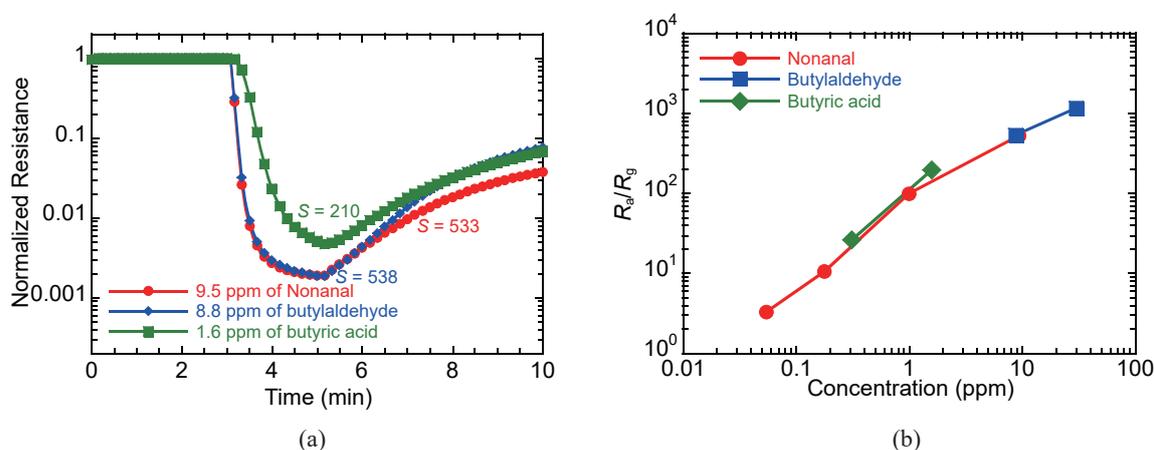

Fig. 6.   (Color online) (a) Dynamic resistance response to 9.5 ppm nonanal, 8.8 ppm butylaldehyde, and 1.6 ppm butyric acid, and (b) sensor response values *S*, of the "advanced-aging" Pt, Pd, Au/SnO$_2$ sensor element. The temperature of the sensor element was 250 °C.

Table 2
Resistance recovery rates [*P*(*t*)] of the "advanced-aging" Pt, Pd, Au/SnO$_2$ sensor elements after 300 s.

Target gas	P(300) (%)
9.5 ppm nonanal	3.6
8.8 ppm butylaldehyde	7.5
1.6 ppm butyric acid	6.4

shown in Table 2. This suggests that the desorption of butyric acid from the SnO_2 system is slower than that of butyraldehyde.

The sensor response curves from the aldehyde gases versus concentration lie almost on a single straight line on the log–log plot in Fig. 6(b), from low-concentration nonanal to high-concentration butyraldehyde, although their resistance recovery rates are different. The *S*-curve from butyric acid also falls on this line.

Figure 7 shows the MS spectra from TPRe analysis at different sample temperatures. In the case of butyraldehyde [Fig. 7(a)], increasing the sample powder temperature suppresses the MS peaks from butyraldehyde (*e.g.*, $m/z = 57$ and 72)[26] and increases those from carbon dioxide ($m/z = 22$ and 44). The MS peaks from butyraldehyde were decreased by heating up to 250 °C, and disappeared at over 300 °C. Interestingly, new peaks at $m/z = 60$ and 73 appeared around the sensor working temperature of 200–350 °C. From the MS patterns, these peaks are those of butyric acid,[26] indicating that the aldehyde group is oxidized to the carboxyl group at the sensor working temperature (250 °C). In the case of isoprene, MS peaks from isoprene (*e.g.*, $m/z = 53$ and 68)[26] decreased and disappeared at over 300 °C, and those from carbon dioxide increased. No peaks belonging to intermediate products were observed.
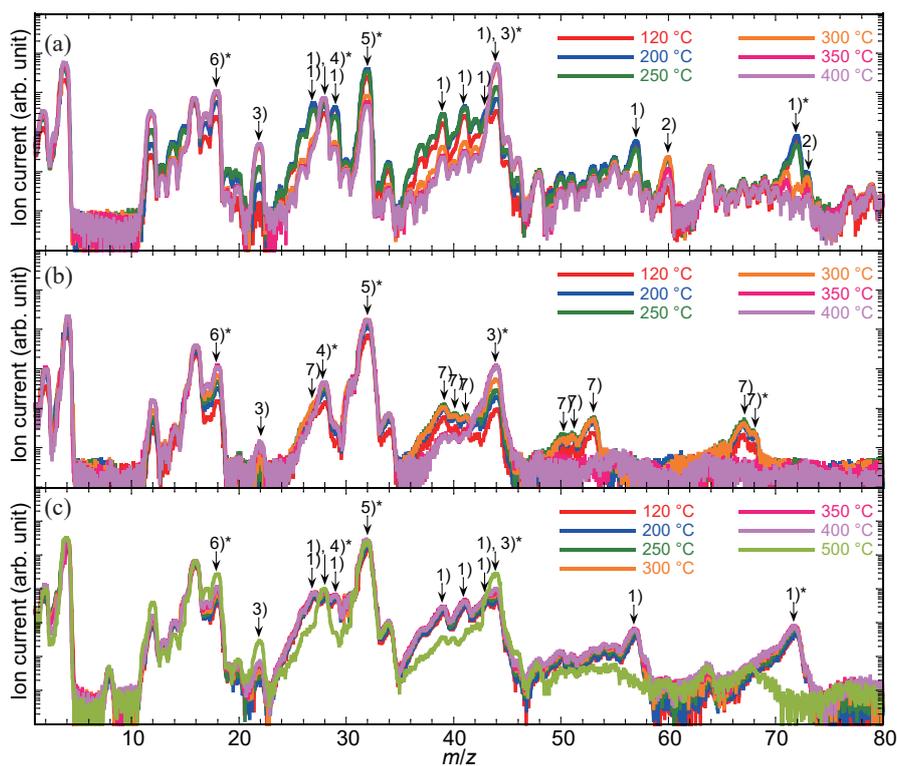

Fig. 7. (Color online) MS spectra from TPRe analysis using Pt, Pd, Au/SnO_2 and pristine SnO_2 sample powders at different temperatures: (a) Pt, Pd, Au/SnO_2 and 1.8×10^3 ppm butylaldehyde, (b) Pt, Pd, Au/SnO_2 and 2.0×10^3 ppm isoprene, and (c) pristine SnO_2 and 1.8×10^3 ppm butylaldehyde. The labeled main peaks correspond to 1) butylaldehyde (C_3H_7CHO), 2) butyric acid ($C_3H_7CO_2H$), 3) carbon dioxide (CO_2), 4) carbon monoxide (CO), 5) oxygen (O_2), 6) water (H_2O), and 7) isoprene (C_5H_8). The asterisks denote the molecular ion peaks.

For comparison, pristine SnO_2 was also investigated in the TPRe study. Pristine SnO_2 hardly oxidizes butyraldehyde at the sensor working temperature, since the MS spectra barely changed up to 400 °C and no butyric acid peaks were observed. Therefore, the loaded noble metal catalysts were responsible for oxidizing the aldehyde group on the SnO_2 surface at the sensor working temperature.

Figure 8 shows the TPRe patterns of target gases and their oxidization products. The TPRe patterns are based on the MS peaks of $m/z = 22$ (carbon dioxide), 57 (butyraldehyde), and 60 (butyric acid) when using butyraldehyde as the target gas, because the molecular ion peaks of butyraldehyde ($m/z = 72$) and carbon dioxide ($m/z = 44$) are affected by the fragment ion peaks of butyric acid and butyraldehyde, respectively, and the molecular ion peak of butyric acid ($m/z = 88$) is hardly observed. When using isoprene as the target gas, the molecular ion peaks of $m/z = 44$ (carbon dioxide) and 68 (isoprene) are used. The increase and decrease in ion currents are related to the concentrations of gases. At low temperature, the ion currents from the target gases (butyraldehyde or isoprene) and carbon dioxide were observed to increase gradually with temperature, indicating that the target gases absorbed at room temperature onto Pt, Pd, Au/SnO_2 are released and oxidized

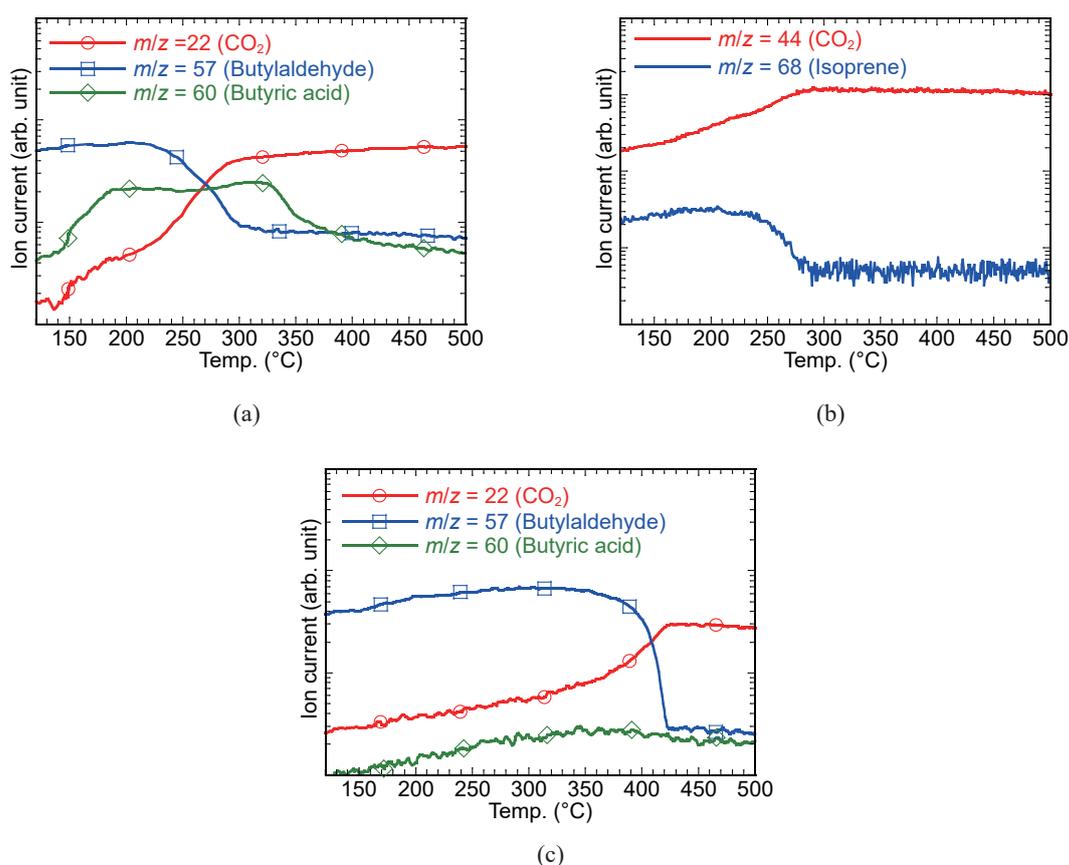(a)   (b)

(c)

Fig. 8.   (Color online) TPRe patterns of the target gases and their oxidization products (CO_2 and butyric acid). The powder samples and target gases are (a) Pt, Pd, Au/SnO_2 and 1.8×10^3 ppm butylaldehyde, (b) Pt, Pd, Au/SnO_2 and 2.0×10^3 ppm isoprene, and (c) SnO_2 and 1.8×10^3 ppm butylaldehyde.

with increasing temperature. The target gas concentrations were drastically reduced at around the sensor working temperature of 250 °C, and all target gas molecules were oxidized over 300 °C, as shown in Figs. 8(a) and 8(b). Figure 9 shows the reaction pathways of the target gases on the sensor materials from the TPRe study. In the case of butyraldehyde, its oxidization intermediate, butyric acid, was observed until 350 °C, which included the sensor working temperature (250 °C). At higher temperatures, over 350 °C, butyraldehyde was oxidized completely to carbon dioxide. Therefore, the sensor responses, i.e., decreased resistance, should relate to the oxidation of target gases on the surface of sensor materials. The Pt, Pd, Au/SnO$_2$ sensor showed a strong response to nonanal (Fig. 4) and butyraldehyde (Fig. 6) but not to isoprene (Fig. 4), indicating that the oxidation of the aldehyde group and the generation of acid significantly decreased the resistance. Isoprene was oxidized completely to carbon dioxide at temperatures exceeding 300 °C. The pristine SnO$_2$ could not oxidize butyraldehyde at the sensor working temperature, and the intermediate product, butyric acid, was hardly observed at all temperatures. At around 420 °C, butyraldehyde was found to oxidize completely to carbon dioxide.

3.3 TEM observation of metal dispersion

Figure 10 shows the TEM, STEM-HAADF, and STEM-EDS images of non-aged and aged Pt, Pd, Au/SnO$_2$ powders. The particle size of Au was larger than that of the original Au colloid particles. In the Pt, Pd, Au/SnO$_2$ system, the Au particles are expected to gather into trimetallic grains during paste annealing at 500 °C. Therefore, the Au particles in the non-aged and aged samples should not be significantly different. Most of the Pd particles in the aged sample were dispersed, although some formed grains around 10–20 nm in size according to the STEM-EDS results. Some of the Pd were present in the trimetallic grains (*e.g.*, the region ~20 nm in size in the second row of Fig. 10), and Pd-rich grains were also observed elsewhere. The Pd particles and Pd-rich grains in the non-aged Pt, Pd, Au/SnO$_2$ [Fig. 10(a), lower middle panel] were also very similar to those in the aged sample [Fig. 10(b), lower middle panel] However, there is one significant difference in the Pt dispersion between the non-aged and aged samples. Although a small portion of these particles was also gathered in the trimetallic grains, the Pt particles were better dispersed than Pd in the non-aged sample.
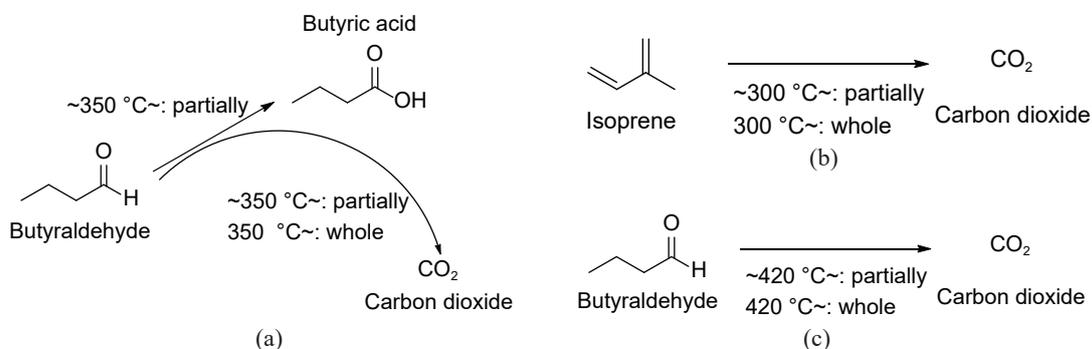

Fig. 9. Reaction pathways of the target gases on the sensor materials from the TPRe study: (a) butylaldehyde on Pt, Pd, Au/SnO$_2$, (b) isoprene on Pt, Pd, Au/SnO$_2$, and (c) butylaldehyde on SnO$_2$.
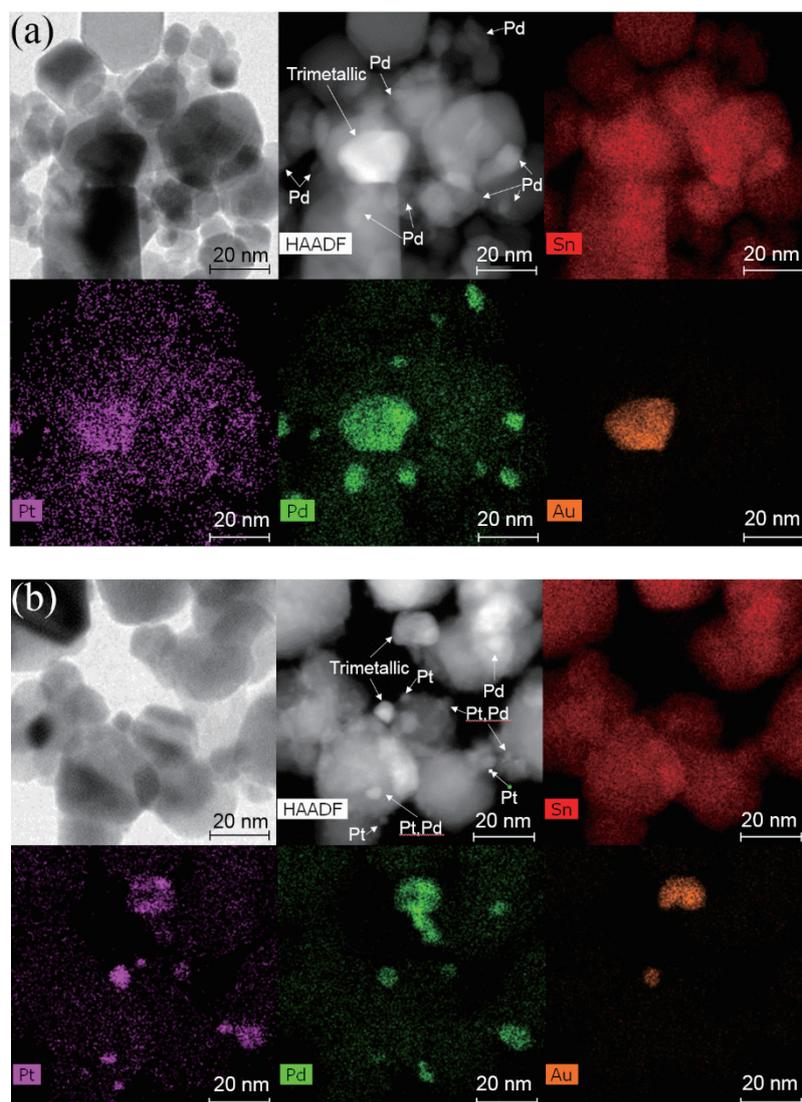
Fig. 10. (Color online) Images of the (a) non-aged and (b) aged Pt, Pd, Au/SnO$_2$ samples, each in the order of: TEM, STEM-HAADF, and STEM-EDS maps of Sn, Pt, Pd, and Au. The magnification of all images is 900000 times.

In the aged sample, the dispersibility of Pt was also reduced, and Pt–Pd bimetallic grains and Pt grains were observed. In the Pt–Pd catalyst system, it has been reported that the noble metal components, namely, platinum oxide and palladium oxide, were converted to bimetallic particles or Pd–Pt core-shell structured grains by aging after annealing at high temperature, and these particles/grains were larger than their initial sizes.[22–24,27] In the Pt, Pd, Au/SnO$_2$ gas sensor system, the aging and local heat generated from VOC oxidation would induce the grain growth of Pt and Pd. Thus, the VOC sensing properties of the Pt, Pd, Au/SnO$_2$ system would depend on the dispersibilities of the noble metal particles.

3.4 Models of the effects of aging on recovery time

Since three noble metals are mixed in the Pt, Pd, Au/SnO$_2$ system, it is difficult to distinguish the catalytic performance of individual metals and/or their alloys. However, a rough mechanism for the sensor response can be deduced from the above results. The Pt, Pd, and Au/SnO$_2$ exhibits deep electron depletion. The resistance at the SnO$_2$ grain boundary is increased by the loaded noble metals, especially Pd.[28] The oxidized Pd affects the electron-depletion layer by electron sensitization.[28] The resistance of Pt, Pd, Au/SnO$_2$ is higher than that of pristine SnO$_2$, because the loaded SnO$_2$ has a much lower density of carrier electrons. The deep electron depletion should be promoted by oxygen adsorption on the SnO$_2$ grains as well as on the oxidized Pd. When the target gas molecules are oxidized with the adsorbed oxygen, the density of carrier electrons increases, causing a sensor response, i.e., a reduction in the resistance of SnO$_2$. In other words, a strong sensor response is obtained by changing from a much lower to a higher carrier electron density. If the slow resistance recovery can be related to the slow restoration from the higher to the much lower carrier electron density, then the recovery time should be independent of the target gases. However, the opposite was observed here. For example, according to Figs. 3(a) and 3(b), and Table 1, the resistance recovery rate after exposure to 0.18 ppm nonanal was much lower than that after exposure to 1.0 ppm isoprene [$P(300) = 32\%$ vs $t_{10} = 212$ s] despite their almost equal response values ($S = 3.6$ vs 3.8). Therefore, the recovery time does depend on the target gases for these sensor elements. For example, residues such as adsorbed target gas molecules on SnO$_2$ could slow the recovery process, by delaying the restoration of oxygen adsorbates.

On the basis of the results obtained here, we propose separate models of Pt, Pd, Au/SnO$_2$ grains exposed to nonanal before and after aging, as shown in Figs. 11(a) and 11(b) respectively, based on the oxidation and adsorption of nonanal molecules. According to Fig. 10(a), Pt and Pd particles, specifically Pt, were well dispersed in the non-aged Pt, Pd, Au/SnO$_2$. Their response to nonanal was low and the recovery afterwards was faster than that in the aged Pt, Pd, Au/SnO$_2$ sample. Therefore, most of the nonanal would be oxidized to nonanoic acid, part of which would be further oxidized by the dispersed noble metals to products, such as carbon dioxide and aliphatic hydrocarbons. Grains of Pt, Pd alloy were generated not only by agglomeration during annealing but also during aging, as shown in Fig. 10(b). These grains would further induce the oxidation
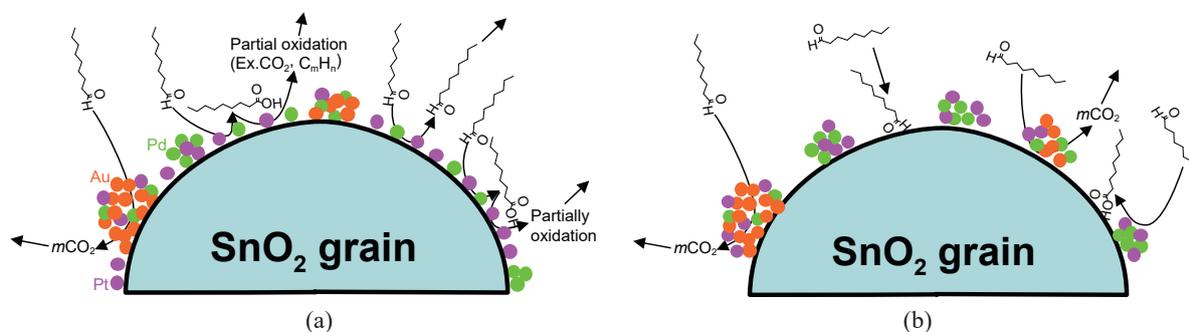

Fig. 11. (Color online) Models of Pt- Pd- and Au-loaded SnO$_2$ grains (a) before and (b) after aging, and nonanal sensing mechanism from the oxidation and adsorption of nonanal molecules.

of VOCs, i.e., carbon dioxide. This would explain the increased sensor response in the aged sample. The aggregation of the noble metal particles, specifically Pt, would increase the area of the "pristine" SnO_2 surface, as shown schematically in Fig. 11(b). In this case, parts of nonanal and its oxidization product (nonanoic acid) would adsorb onto the "pristine" SnO_2 surface. These adsorbed molecules can interfere with oxygen readsorption after exposure, and/or donate electrons to SnO_2 from the aldehyde or carboxylic acid groups, as shown in Fig. 11(b). The slow desorption of nonanoic acid from the surface of SnO_2 means that it takes longer to restore the depletion layer, leading to the observed slower recovery after nonanal exposure.

4.   Conclusions

The Pt, Pd, Au/SnO_2 sample pretreated by aging showed a stronger sensor response to nonanal at 250 °C, but a longer recovery time after nonanal exposure, while it showed a short recovery time after isoprene exposure. From the TPRe study, a portion of isoprene was oxidized to carbon dioxide on the sensor material. When using butyraldehyde, which consists of an aldehyde group and a straight alkyl chain similar to nonanal, the target gas was oxidized to butyric acid at the sensor working temperature of 250 °C. TEM observation indicates that Pt and Pd particles, specifically Pt, were well dispersed in the non-aged Pt, Pd, Au/SnO_2. In the aged sample, the dispersibility of Pt was reduced, and Pt–Pd bimetallic grains and Pt grains were formed. On the basis of these results, we propose models of the effects of nonanal gases on the resistance of the Pt, Pd, Au/SnO_2 sensor element. On the aged Pt, Pd, Au/SnO_2, nonanal would be partially oxidized to nonanoic acid, some of which would adsorb on the SnO_2 surface together with residual nonanal, and decrease the resistance of the sensor by interfering with the oxygen adsorption on the surface and/or donating electrons to SnO_2 from the aldehyde and carboxylic acid groups. The slower recovery time after nonanal exposure compared with the non-aged sample could then be explained by the slow desorption of nonanoic acid from the surface of SnO_2 in the former.

References

1   Z. Li, Q. Zhao, W. Fan, and J. Zhan: Nanoscale **3** (2011) 1646.
2   Z. Wen and L. Tian-mo: Physica B **405** (2010) 1345.
3   N. Yamazoe and K. Shimanoe: Sens. Actuators, B **128** (2008) 566.
4   N. Yamazoe and K. Shimanoe: Sens. Actuators, B **138** (2009) 100.
5   M. Kadosaki, Y. Sakai, I. Tamura, I. Matsubara, and T. Itoh: Electro. Commun. Jpn. **93** (2008) 34.
6   Y. Sakai, M. Kadosaki, I. Matsubara, and T. Itoh: J. Ceram. Soc. Jpn. **117** (2009) 1297.
7   T. Itoh, I. Matsubara, M. Kadosaki, Y. Sakai, W. Shin, N. Izu, and M. Nishibori: Sens. Mater. **21** (2009) 251.
8   T. Itoh, I. Matsubara, M. Kadosaki, Y. Sakai, W. Shin, N. Izu, and M. Nishibori: Sensors **10** (2010) 6513.
9   M. Greabu, A. Totan, D. Miricescu, R. Radulescu, J. Virlan, and B. Calenic: Antioxidants **5** (2016) 3.

10   Y. Yasuno, M. Iwakura, and Y. Shimada: J. Dental Health **39** (1989) 663.

11   M. Kishi, Y. Ohara-Nemoto, M. Takahashi, K. Kishi, S. Kimura, F. Aizawa, and M. Yonemitsu: Arch. Oral Biol. **58** (2013) 324.

12   D. Gelmont, R. A. Stein, and J. F. Mead: Biochem. Biophys. Res. Commun. **99** (1981) 1456.

13   C. Wang, A. Mbi, and M. Shepherd: IEEE Sensors Journal **10** (2010) 54.

14   J. King, H. Koc, K. Unterkofler, P. Mochalski, A. Kupferthaler, G. Teschl, S. Teschl, H. Hinterhuber, and A. Amann: J. Theoret. Biol. **267** (2010) 626.

15   J. King, P. Mochalski, K. Unterkofler, G. Teschl, M. Klieber, M. Stein, A. Amann, and M. Baumann: Biochem. Biophys. Res. Commun. **423** (2012) 526.

16   D. Poli, P. Carbognani, M. Corradi, M. Goldoni, O. Acampa, B. Balbi, L. Bianchi, M. Rusca, and A. Mutti: Respir. Res. **6** (2005) 71.

17   P. Fuchs, C. Loeseken, J. K. Schubert, and W. Miekisch: Int. J. Cancer **126** (2010) 2663.

18   G. Song, T. Qin, H. Liu, G.-B. Xu, Y.-Y. Pan, F.-X. Xiong, K.-S. Gu, G.-P. Sun, and Z.-D. Chen: Lung Cancer **67** (2010) 227.

19   M. Hakim, Y. Y. Broza, O. Barash, N. Peled, M. Phillips, A. Amann, and H. Haick: Chem. Rev. **112** (2012) 5949.

20   K. D. van de Kant, L. J. van der Sande, Q. Jöbsis, O. C. van Schayck, and E. Dompeling: Respir. Res. **13** (2012) 117.

21   T. Itoh, T. Nakashima, T. Akamatsu, N. Izu, and W. Shin: Sens. Actuators, B **187** (2013) 135.

22   G. W. Graham, H.-W. Jen, O. Ezekoye, R. J. Kudla, W. Chun, X. Q. Pan, and R. W. McCabe: Catal. Lett. **116** (2007) 1.

23   M. R. Ward, T. Hyde, E. D. Boyes, and P. L. Gai: ChemCatChem **4** (2012) 1622.

24   M. Honkanen, M. Kärkkäinen, V. Viitanen, H. Jiang, K. Kallinen, M. Huuhtanen, M. Vippola, J. Lahtinen, R. Keiski, and T. Lepisto: Top. Catal. **56** (2013) 576.

25   H. Sakurai, T. Akita, S. Tsubota, M. Kiuchi, and M. Haruta: Appl. Catal., A **291** (2005) 179.

26   SDBSWeb: http://sdbs.db.aist.go.jp (National Institute of Advanced Industrial Science and Technology, accessed 23 Februaly 2016).

27   A. Morlang, U. Neuhausen, K. V. Klementiev, F.-W. Schütze, G. Miehe, H. Fuess, and E. S. Lox: Appl. Catal., B **60** (2005) 191.

28   S. Matsushima, T. Maekawa, J. Tamaki, N. Miura, and N. Yamazoe: Sens. Actuators, B **9** (1992) 71.